Gain Stabilization in POLAR-2 SiPMs Using Temperature Loop Corrections

Trevor Hennington[1], *Mobin Mobaseri*[2]
Supervisors: Johannes Hulsman[2], *Vishal Kumar*[2]
[1]CERN, Geneva, Switzerland
[2]University of Geneva, Geneva, Switzerland

Abstract

Gamma-Ray Bursts (GRBs) are among the most extreme events in the universe, however much is yet to be understood about the structure of their outflows, magnetic characteristics, and kinetic energy. Knowing the polarization of light coming from GRBs is expected to help solve some of these open questions. POLAR-2 is a future space-based GRB detector which will measure the polarization of incoming photons from extragalactic sources. It will use Compton Scattering in scintillator bars that are read out by Silicon Photomultipliers (SiPMS) for these measurements. However, the characteristics of SiPMs are highly dependent on temperature, in particular their gain is inversely proportional to temperature assuming a constant bias voltage. During operation, POLAR-2 will be subject to extreme temperature changes in space, so if a constant gain is desired the bias voltage will need to be corrected. In this study, a temperature correction loop for the bias applied to the SiPMs in a POLAR-2 module was studied and characterized. Its performance was investigated by measuring the gain of the module's SiPMs across a range of temperatures from 20 to 34 °C. The results were compared against control data without a temperature correction. The correction loop was determined to be effective but not ideal, as a dependence on the order of -0.2 per °C was observed in the gain of many SiPM channels. An improvement to the correction loop was made, and the mean temperature dependence went from -0.07 to -0.04 per °C. However, a dependence on the order of -0.2 per °C was still observed in many SiPM channels. It was determined that the temperature loop correction is effective at reducing temperature dependence of SiPM gain, but that further optimizations may be desired.

Keywords
POLAR-2; Gamma-Ray Bursts (GRBs); Polarization; Scintillators; Compton Scattering; Silicon Photomultipliers (SiPMs); Gain; Temperature Correction Loop.

Contents

1 Introduction

POLAR-2 is a manifested Gamma-Ray Burst (GRB) space-based polarimeter succeeding the POLAR [1] mission with a broader range in energy and increased effective measurement area [2]. The main improvements of POLAR-2 when compared to POLAR is its usage of Silicon Photomultipliers (SiPMs) rather than the Multi-Anode Photo Multiplier Tubes, an increase in number of modules from 25 to 100, an increase in scintillator volume, and the use of wrapped scintillators [3].

The polarimeter utilizes the effects of Compton Scattering in plastic scintillator bars to measure the polarity of incoming gamma-rays. A gamma-ray will deposit some energy into a scintillator bar, scatter to another bar, and deposit energy again. Then scintillation light in the bars are read out by the SiPMs [4]. A diagram of this process is illustrated in Figure 1. The angular distribution of photon hits can then be used to determine the polarization of the source [2].

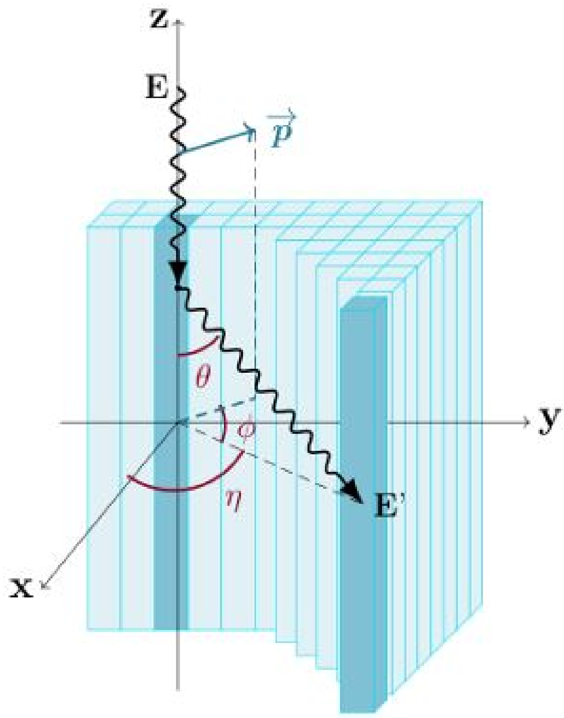

Figure 1: Compton scattering of an incoming photon from one scintillator bar to another [2].

Once completed, the POLAR-2 instrument will consist of 100 polarimeter modules in a 10x10 grid. Each module contains 64 scintillator bars in an 8x8 grid and 4 SiPM arrays (each SiPM array has 16 channels, totaling 64 in an 8x8 grid) [4]. These are encased in a carbon fiber socket for light tightness and shielding of low energy particles to block external sources not produced by GRBs. Figure 2 shows a detailed diagram of the module's parts expanded out for reference.

Not included in the diagram are three NTC thermistors (NTC0, NTC1, and NTC2), installed on the back of the SiPM arrays and the Front End Electronics (FEE) to measure temperature (three are needed to measure a temperature gradient [5]). These work by measuring the resistance of the NTC and reading it out as a 12-bit ADC value. The conversion from ADC to temperature is shown in Equation 1 [6].

$$T[^{\circ}C] = \frac{3435}{\ln\left[\frac{\frac{3.3*25500}{1.6+(ADC_{NTC}/4095*3.3-1.6)/1.2}-25500}{10000}\right] + \frac{3435}{298.15}} - 273.15 \tag{1}$$

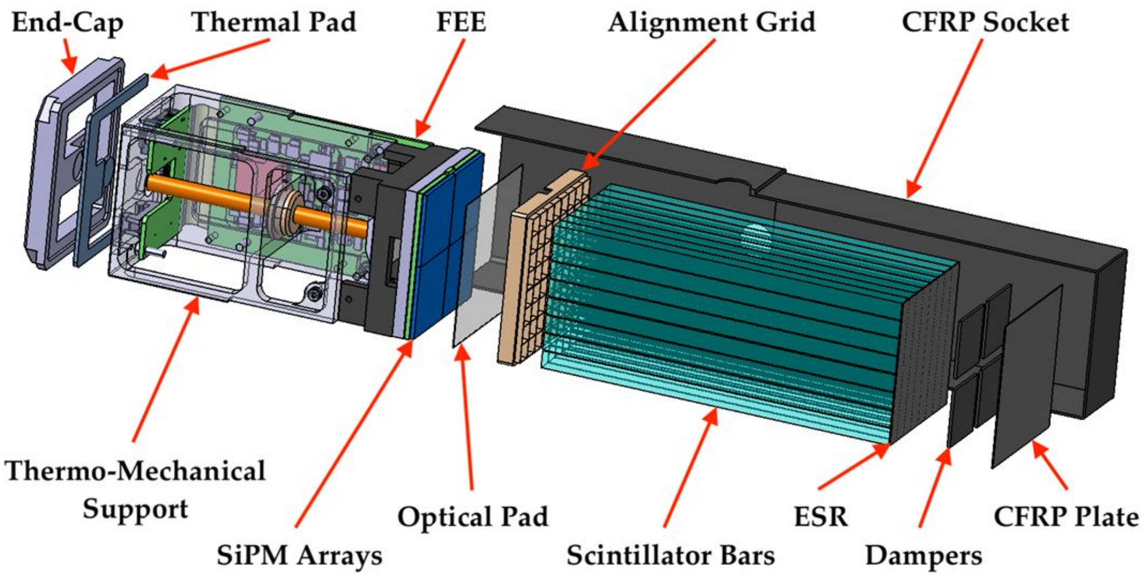

Figure 2: Exploded view of a POLAR-2 module [4].

1.1 Temperature Correction with the HV-table

The main drawback of using SiPMs is that the dark current is highly dependent on temperature. Therefore, if a constant gain is desired regardless of temperature, the bias voltage supplied must be adjusted accordingly.

The solution to this is a temperature correction loop, which is continuously applied during data acquisition and is referred to as the "HV-table". The HV-table works by reading the NTCs at the beginning of every loop, and then using a weighted average of the three NTCs to index an 8-bit lookup table. However, since the NTC's ADC value is 12-bit, only the eight most significant bits are used to index the table. Each table index corresponds to a 9-bit (8-bit with sign) correction value, which is then applied to the input bias voltage (a 12-bit value referred to as the "HV").

1.2 Experimental Goals

The goal of this study is to characterize the functionality of the HV-table using the POLAR-2 EQM1 module at CERN. First, it had to be verified that the HV-table correction was being properly applied in the Front End Electronics (FEE). Once this was confirmed, the relationship between temperature and the gain of the SiPMs needed to be measured both with and without the use of the HV-table. If it was determined that improvements were needed to keep the gain of the module's SiPMs constant with changing temperatures, a new HV-table was should be generated, tested, and compared to the original table.

2 Experimental Setup

The tests were done with the Engineering Qualification Module 1 (EQM1) at CERN and a Zynq electronics board, as shown in Figures 3 and 4. The EQM1 module is designed to be space qualified but will only be used for Earth-based testing. Power is delivered to the module from the Zynq board which itself receives power from a connected PC through USB-C. The Zynq board also has a LAN and micro USB connection to the PC. Additionally, the EQM1 module being tested at CERN had an Am-241 radioactive source installed within for characterization.

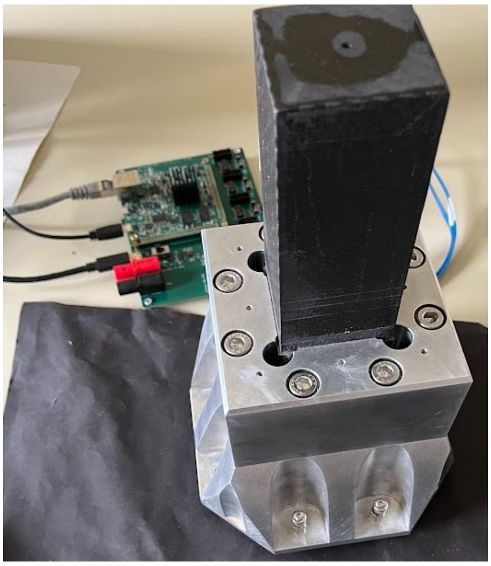

Figure 3: EQM1 module at CERN.

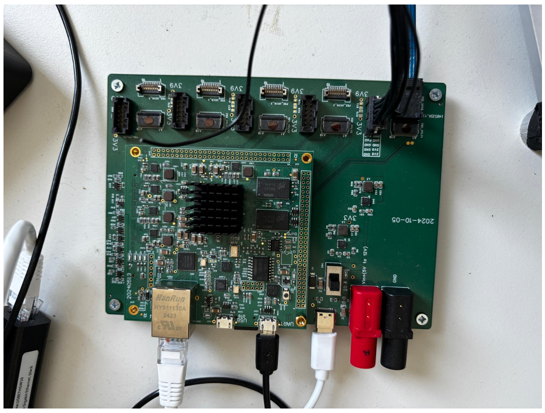

Figure 4: Zynq electronics board.

2.1 Data Acquisition

The Zynq board can run data acquisition scripts and then data is sent back to the PC as .root files. This is done by connecting to the Zynq from the PC using SSH protocol, running a command on the PC to begin saving the data, and pushing a command to the Zynq to execute the DAQ script. The DAQ script has some options when being ran: the amount of time to collect data in seconds, the voltage bias (HV), if housekeeping data (temperature, current, voltage, etc.) is recorded, and the configuration file to be used.

The configuration file must first be uploaded to the Zynq and further specify parameters to be set during the data acquisition. Most notably, these parameters include the thresholds for both charge and time counts, gain corrections for individual SiPMs, and, most importantly for this study, the HV-table values.

As previously discussed in Section 1.1, a loop in the DAQ script reads the temperature from the NTCs, indexes the HV-table, adds the corresponding value to the HV set when the DAQ script was first executed, and then sets this new total HV as the input bias voltage to the module's SiPMs. This loop repeats at a frequency of 0.5 Hz [6].

2.2 Data Analysis

Specifically, a POLAR-2 script was used for quickly inspecting a data file to determine if a significant number of events were captured without also having too much noise. Some example plots output from this script are shown in Figures 5 and 6.

Figure 5 shows an example output of the "2D charge trigger pattern plot", which shows the hit rate for a .root file that was passed through the analysis script. The grid represents each SiPM channel as they are physically arranged in the detector. The numbers in each square give the total number of counts in the SiPM channel that were above the set charge trigger threshold.

In the example hit rate plot, the location of the Am-241 source can be seen at the SiPM channel with the highest count rate in yellow. This is what the charge trigger pattern is expected to look like, so any data files that did not match this were discarded. For example, a data file with too much noise would have high count rates in channels far from the source. Alternatively, in a file with too high a threshold, the source would not be distinguishable.

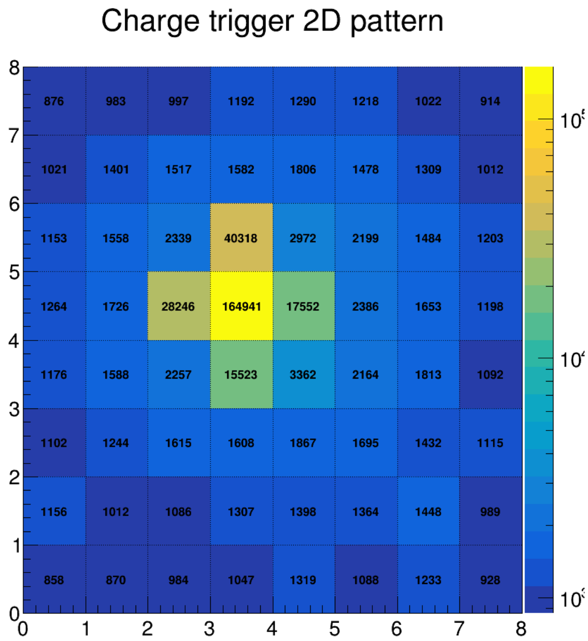

Figure 5: Example plot of charge trigger pattern where the radioactive source is clearly visible.

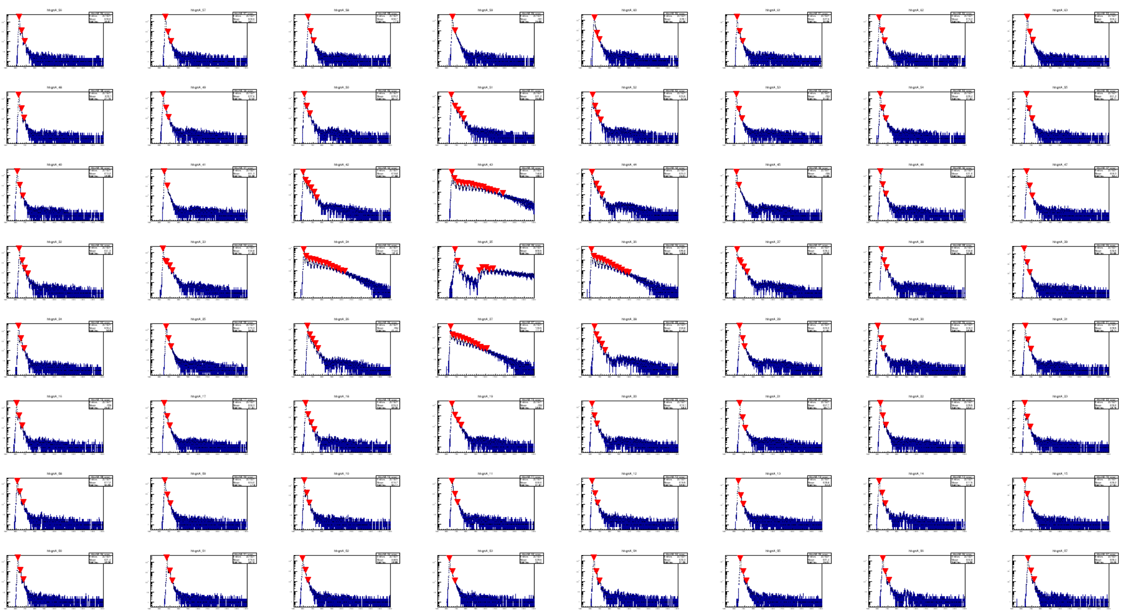

Figure 6: Example finger plots.

Figure 6 shows an example output of the "finger plots" for each channel, which histograms the detected ADC values. This helps to visualize at what energies each channel was primarily receiving events.

The red triangles mark where a peak was identified. These peaks correspond to the number of photoelectrons received during that count. The first peak measures the pedestal value, the second peak one photoelectron, the third peak two photoelectrons, etc. The first few peaks in each channel correspond to noise, while a peaks corresponding to a higher number of photoelectrons represent where real signal is detected, which can be visually seen in the plots where the Am-241 source is installed. Ideally, each SiPM has enough peaks so that a linear fit can be applied to the ADC value vs photoelectron number.

Additionally, dedicated scripts [7] were developed to automate the process of analyzing the performance of the HV-table and creating an HV-table. The scripts follow the steps described in the following sections and are capable of producing the plots shown.

3 HV-table Characterization

The gain in a SiPM channel is given by the total number of charge released during an avalanche in the avalanche photo-diodes (APDs).

$$G \simeq \frac{(V_{bias} - V_{bd}) \cdot C_j}{e} \tag{2}$$

Where V_{bias} is the reverse bias voltage applied (High Voltage (HV)), V_{bd} is the breakdown voltage, C_j is the junction capacitance, and e is the electric charge unit[1]. If V_{bias} is set to be equal to V_{bd}, the field in the depletion region is just at the edge of avalanche breakdown. Therefore, to trigger an avalanche, V_{bias} (the HV) needs to be more than V_{bd}.

As mentioned, the gain is a function of temperature; we need to know where this dependence comes from. In Equation 2, we have $\Delta V = V_{bias} - V_{bd}$ and C_j, which are both functions of temperature. However, the change in C_j with respect to temperature is negligible [8], therefore any temperature dependence of the gain comes from ΔV.

If the breakdown voltage is approximated to be linear with temperature, then

$$V_{bias} = V_{bias,0} + \frac{dV_{bd}}{dT} \cdot (T - T_{ref,0}) \tag{3}$$

Where the index 0 indicates the reference temperature.

During data collection, the initial bias, $V_{bias,0}$, is set when initializing the DAQ command, and the HV-table adds the temperature correction. The HV-table is defined as being 0 at the reference temperature ($0\ ^\circ C$), giving the following

$$V_{bias} = V_{bias,0} + HVtable \tag{4}$$

If we wish to maintain a constant gain with respect to temperature, a correction voltage should be applied. Then, from Equations 3 and 4 it can be seen that

$$HVtable = \frac{dV_{bd}}{dT} \cdot T \tag{5}$$

This is the correction voltage, which we call HVTable. The HV-table function is then digitized into 256 values to cover a range of possible temperatures.

First, it had to be confirmed that the correction from the HV-table was actually being added to the input bias. This was tested by taking data while the values in the HV-table were set to 0. Second, the HV-table was set to a constant value, and the initial bias ($V_{bias,0}$) was decreased by an equal amount. These measurements were made at the same temperature to exclude the effect of temperature on gain. This ensured that both measurements should have the same total bias as given in Equation 4 and therefore the same gain.

The gain was compared for these measurements and they were observed to be equal, determining that the HV-table is indeed being correctly applied. This test was repeated for different total values of V_{bias} (and therefore different gain) as a further confirmation, shown in Figure 7.

Figures 7a and 7b have different initial biases, but sum to the same total bias when the HV-table is added. The mean gain for is less than one standard deviation apart, indicating the HV-table is being

[1] This is derived from integrating the amount of charge released in a SiPM over time per unit charge at reference temperature.

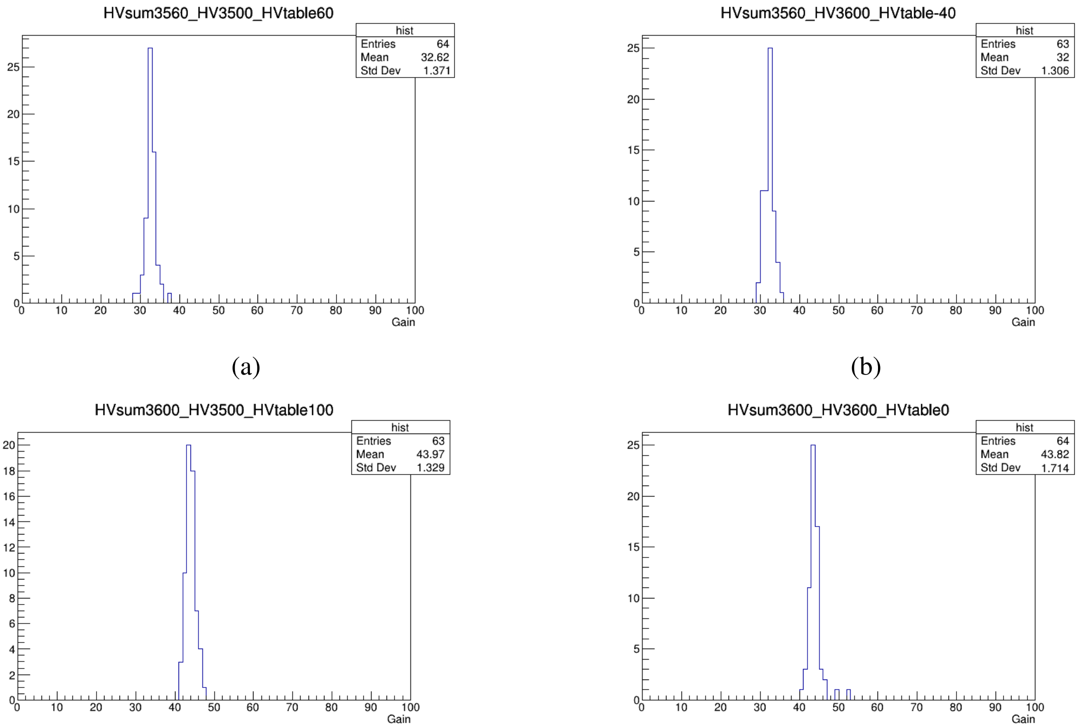

(a) (b) (c) (d)

Figure 7: Histograms of gain in all 64 channels for different initial biases (HV) and HV-tables values.

correctly added. Figure 7c has the same initial bias as 7a but a different HV-table value, and the mean gains are not equal (This can also be said for Figures 7d and 7b), providing further evidence to support this conclusion.

3.1 Data Collection

Currently, our experimental setup does not allow for external control of the module's temperature, but the module has a tendency to slowly heat up during the course of use. This behavior was taken advantage of to collect a set of 40 .root files with the HV-table ranging from temperatures of 20.4 to 34.3 °C (according to NTC0). For all data runs, the configuration file was kept unchanged, and the initial HV was set to 3400.

A control data set where all the values of the HV-table were set to zero was also collected in this manner, with temperatures ranging from 19.7 to 29.5 °C. This is needed to be used as a baseline to compare against and to ensure that the HV-table was being applied in the first place. For the control data, the initial HV was set to 3480. This needed to be higher than for the previous data set to get enough counts, as the HV-table is no longer being added to the bias.

The HV values given are in 12-bit DAC units; the conversion from DAC units to voltage is given in Equation 6.

$$V = (3.3 \cdot 22)\frac{DAC}{4096} \tag{6}$$

3.2 Gain Calculation

For calculating the gain, the charge histogram (finger plot) was first created for each channel as shown by the example in Figure 8.

The first is the pedestal (baseline signal), the second peak is the first photoelectron, etc. The peaks are found using an algorithm to find the local maxima; if the peak is within our tolerance spacing (less than 25 percent deviation), they are accepted. Then, a linear fit was performed on a plot of the ADC versus number of photoelectrons. The pedestals with high errors were not counted in the fit, and there must be at least three peaks to perform the fit. The slope of this fit will be equal to the separation between the peaks, which is equivalent to the gain. An example of this fit is shown in Figure 9, in this case, the slope gives a gain of 25.94 ± 1.91.

The above steps were done to calculate the gain for all 64 SiPMs in every data file for both the HV-table and control data sets.

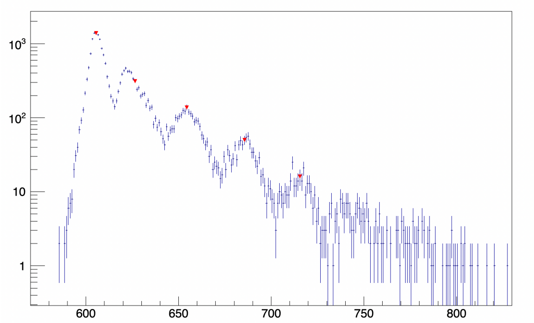

Figure 8: Charge Histogram example, channel 42, file 0.

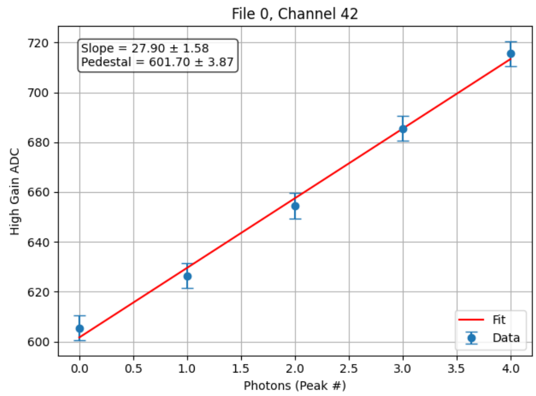

Figure 9: ADC vs number of photoelectrons example, channel 42, file 0.

3.3 Gain vs Temperature

Each .root file contains a list of temperatures read out approximately every second from the NTC modules during the course of the data collection, and the mean of these temperatures was taken as the temperature for that file. Finally, for both the control and HV-table data sets, gain versus temperature plots were generated for 64 channels as shown in Figure 10.

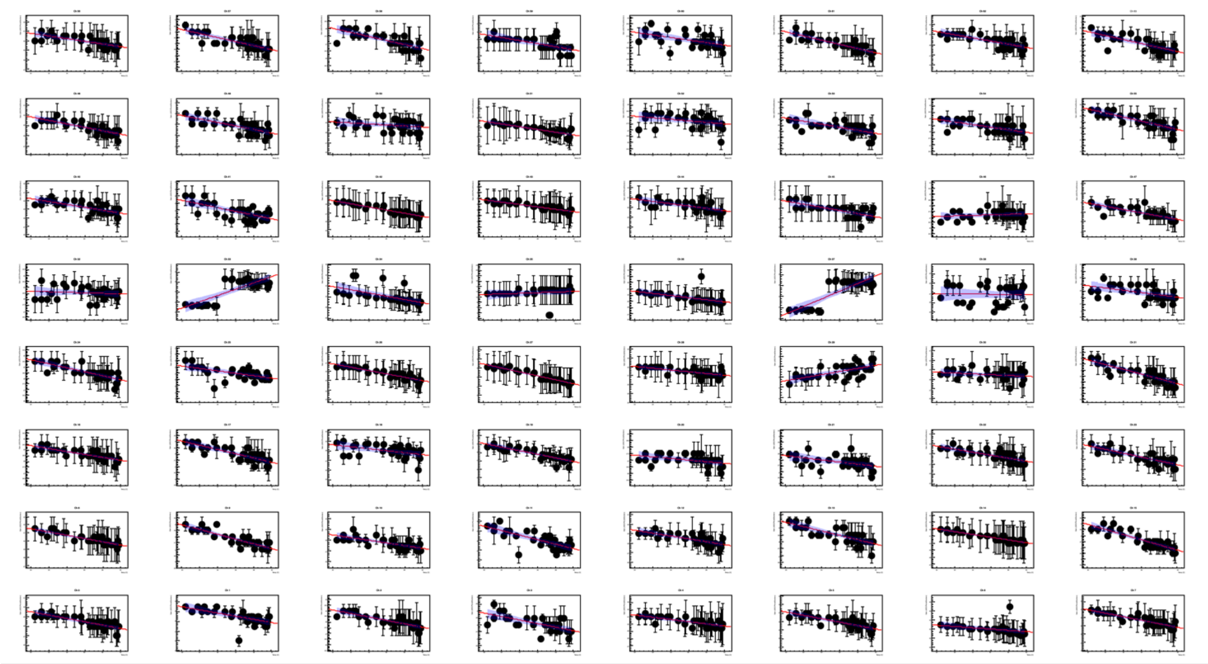

(a) HV-Table added for each temperature.

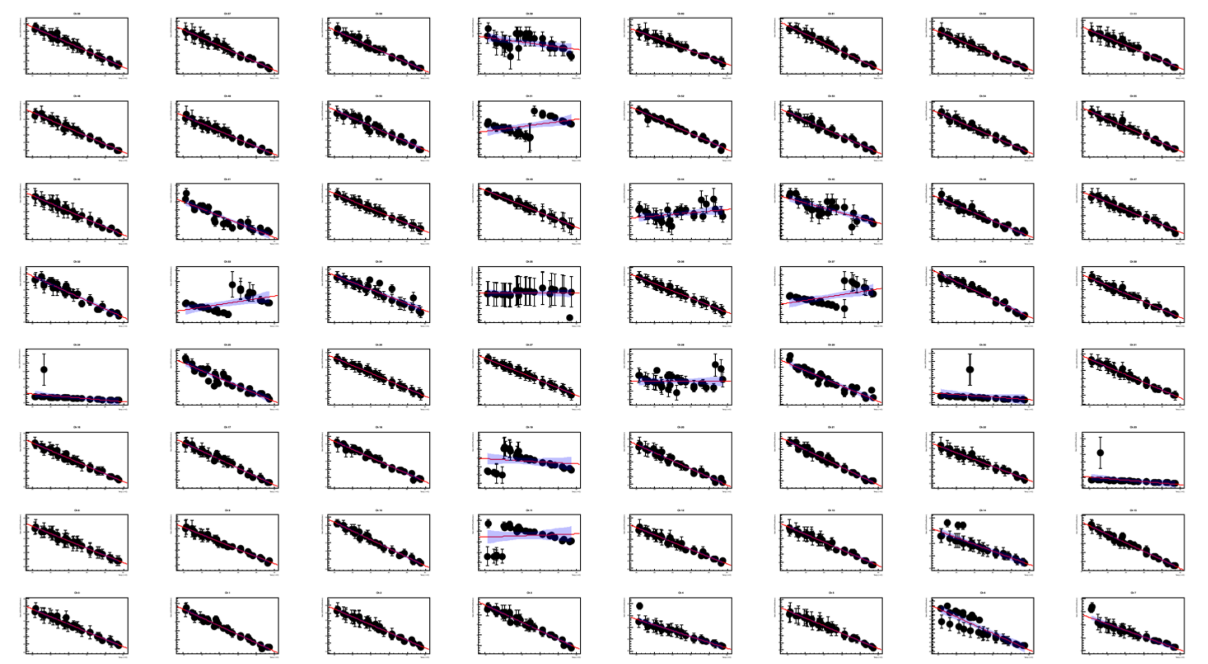

(b) HV-Table set to zero for all temperatures

Figure 10: 64 channel view of gain versus temperature plots for the two scenarios.

A linear fit was performed for every channel, and a confidence band of 95% was included. Only the gain error is taken into account for the linear fit. An example of SiPM channel 42 is shown in Figure 11.

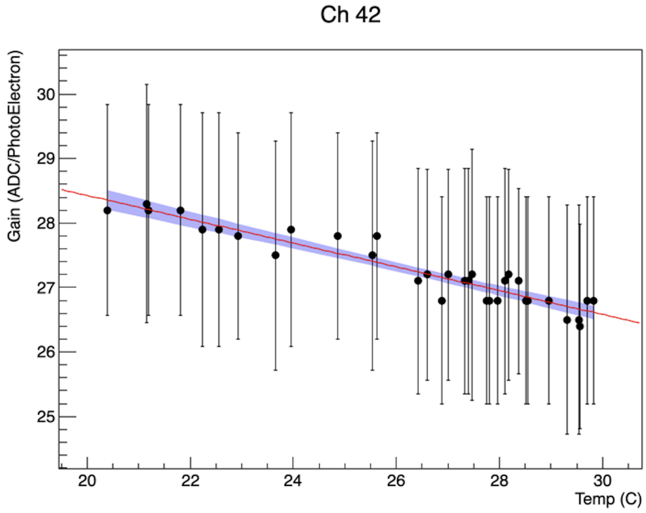

Figure 11: Example of gain vs temperature linear fit for SiPM channel 42 with the confidence band.

3.4 Gain Evaluation

To quantify the performance of the HV-table for all channels, a histogram of the slopes of all 64 channels was made for both the HV-table and control data sets, shown in Figure 12.

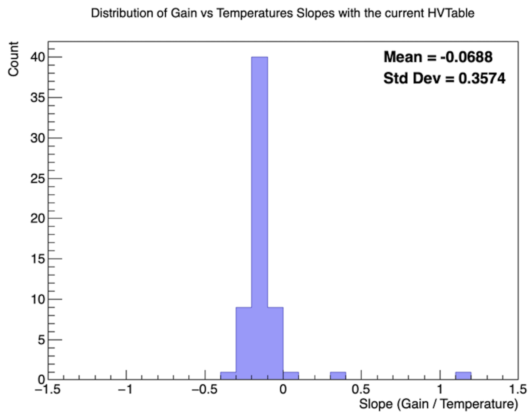

(a) HV-table adjusted case.

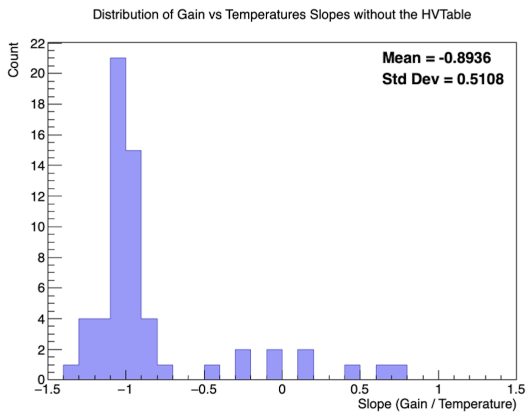

(b) Control case.

Figure 12: Histograms of the slopes of gain versus temperature plots for the two scenarios.

In these histograms, the improvement is evident when comparing the two data sets. The histogram without the HV-table is centered near -1, while with the HV-table the mean is significantly closer to 0. Therefore, on average, the temperature dependence is much less substantial with the HV-table than without it, showing that the HV-table is performing as desired but should still be improved.

4 Attempt to Improve the HV-table

The results in section 3 show a major improvement with the HV-table compared to without it and are a step in the right direction, but ideally, the slope of gain vs. temperature plots should be zero for all SiPMs. In this section, an approach to improve the HV-table using newer SiPM characterization data is detailed.

4.1 Characterizing SiPM Temperature Dependence

Data from the probing of new SiPMs were taken. Each batch of SiPMs was probed at seven temperature points starting from -20 to 40 degrees centigrade in 10-degree intervals. Each batch consists of five trays and each tray is assembled from 24 arrays with 16 SiPM channels. The data we use for this analysis are from batch 114, tray 09 and 10. We later took the data from tray 06, 07, 08, and 10 of the same batch and noticed a difference in potential breakdown between some trays.

The breakdown potential (V_{bd}) for each SiPM was calculated by taking the extrema of the derivative of I-V curves. The V_{bd} for all SiPMs was taken as the mean of the histogram of breakdown potentials of SiPMs shown in Figure 13. After analyzing the data from the trays, we observed that this mean is different for them. This difference should not be significant, and we should be able to merge the data and get a mean V_{bd} for the whole batch; however, there is a difference between the trays. This difference is shown in Figure 14.

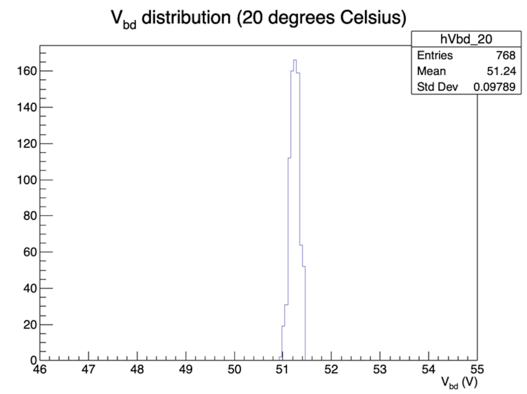

Figure 13: Histogram of breakdown potentials for batch 114, tray 09 and 10

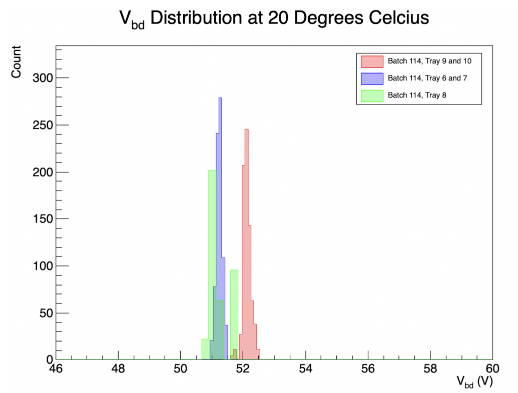

Figure 14: Comparison of the histograms of the breakdown potentials for different trays.

After calculating the V_{bd} at the seven temperature points we can use interpolation to fit the breakdown potential as a function of temperatures. Figure 15 shows the V_{bd} vs temperature plot for tray 06 and 07, 09 and 10, and tray 08. It can be seen that the slopes of the interpolation functions for these three plots are not significantly different; therefore, we conclude that we can merge the trays together.

As mentioned, the following analysis is done on batch 114, tray 09 and 10.

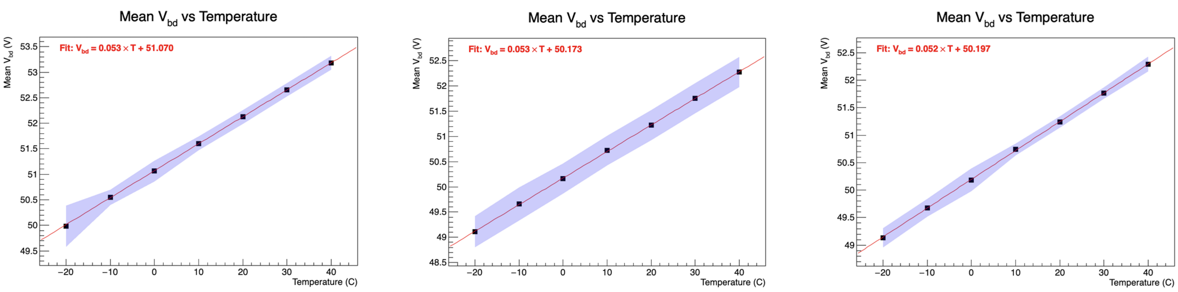

(a) Tray 06 and 07 (b) Tray 08 (c) Tray 09 and 10

Figure 15: Breakdown potential vs temperature plots.

4.2 Creating New HV-table

The 8-bit table index first needs to be translated into the corresponding temperatures. The DAQ script uses the 8 most significant bits of the 12-bit NTC ADC to index the table, so the numbers 0 through 255 were converted to the corresponding 8-bit binary representation, then to 12-bit numbers by simply adding 0000 to the end, and then back to integer values. Finally, the corresponding temperatures are calculated from Equation 1. These 256 temperatures are plugged into the slope from the interpolation of SiPM breakdown potential vs temperature, resulting in the correction values to be placed in the HV-table.

The new and old HV-table are shown plotted as the HV DAC correction against the respective table index in Figure 16. Obviously, the difference between the two tables is very small, so Figure 17 is added to quantify the difference between them.

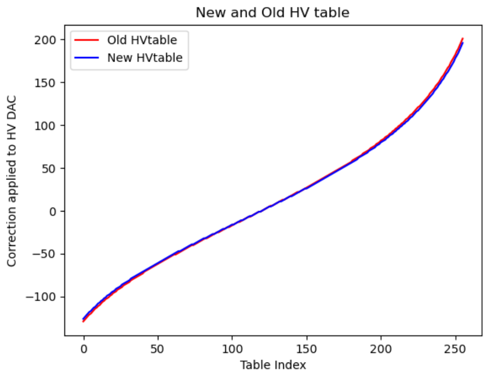

Figure 16: New and Old HV-tables.

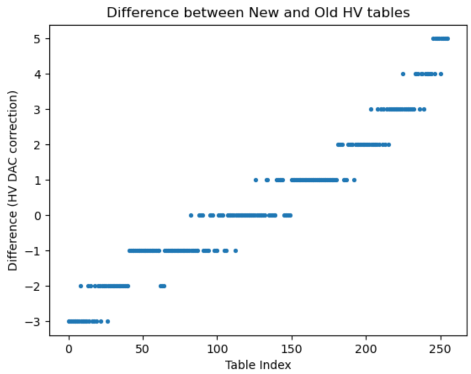

Figure 17: Difference between HV-tables.

The fact that both tables are so similar is both a positive and a negative. It shows that the steps taken to develop the new HV-table were performed correctly (assuming the old table was also developed correctly) and that the method produces consistent results. On the other hand, it is unlikely this new table will show a strong improvement over the previous one. Despite this, the new HV-table was still characterized to determine if such a small change would have a significant impact on the gain.

4.3 Characterizing New HV-table

The same process detailed in section 3 was performed with the new HV-table, resulting in a new data set with 32 .root files ranging from 23 to 28.9 °C. The reason for a smaller range in temperature is due to the data being taken on only one day, while the other data sets were taken on multiple days when the air temperature changed significantly. However, the range of temperatures that were taken is significant.

To visually compare all three data sets, they were plotted together for each channel; an example of which is shown in Figure 18. For SiPM 42, the slopes were identical for both HV-tables. However, some SiPMs did show improvement (such as SiPM 21 which improve from a slope of -0.14 to -0.03), while others did not, or got worse (such as SiPM 46 going from -0.04 to -0.16).

Finally, the histogram of slopes for the new HV-table can be seen in Figure 19. The mean for this new histogram is marginally closer to zero than for the old HV-table. This indicates that on average more SiPMs improved with the new HV-table. However, it is important to note that the standard deviations of the means for both HV-tables overlap.

4.4 Discussion

A potential explanation for the imperfection of both HV-tables is that these corrections were developed from average measurements of SiPM IV-curves. However, since each SiPM array may have slightly

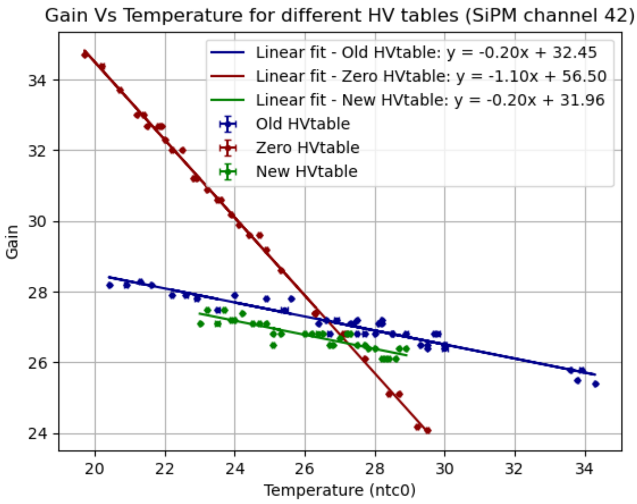

Figure 18: Comparison plot of gain vs temperature in SiPM channel.

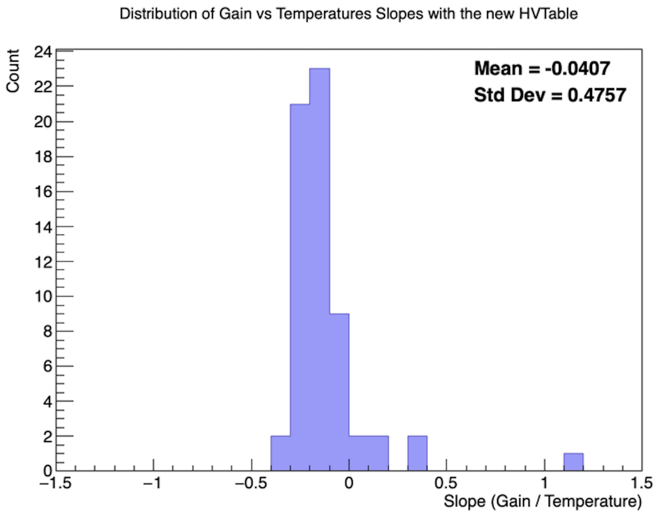

Figure 19: Histogram of the slopes of gain versus temperature plots for the new HV-table.

different characteristics or defects, it may be optimal to carefully recreate configuration files for each module so that their behavior more closely reflects the average. Then the procedures performed in this study should be repeated to characterize the HV-tables performance.

Additionally, only a small batch of SiPM IV-curve data was used to generate the HV-table, so it may be beneficial to use a larger sample size in the future.

5 Conclusions

Since POLAR-2 will be subject to a wide range of temperatures in the environment of space, it is crucial that the effects this will have are accounted for. Otherwise, POLAR-2 will only be able to collect meaningful data for a small fraction of its time in orbit. A method to characterize the temperature loop correction for SiPM bias (or HV-tables) in POLAR-2 modules was developed and tested. Additionally, a new HV-table was generated to improve upon the previously developed HV-table.

It was first observed that the HV-table correction is being properly applied to the bias of the SiPM.

It was then observed that without an HV-table, the gain in most SiPM channels vary on the order of -1 per °C. Both HV-tables were shown to significantly improve this dependence, reducing it to being on the order of -0.2 per °C for most SiPM channels. From the old to the new HV-table, an improvement of the dependence by 0.03 closer to zero was observed. However, this was only for the mean value, and the median remained near -0.2 per °C for both tables.

Acknowledgments

We wish to thank our supervisors, Johannes Hulsman and Vishal Kumar, for guiding us through the learning process of working with the experiment and the equipment being used, and for giving us the opportunity to learn many new skills and data analysis techniques that will doubtless be crucial to our future scientific endeavors.

Bibliography

[1] N. Produit, T.W. Bao, T. Batsch, T. Bernasconi, I. Britvich, F. Cadoux, I. Cernuda, J.Y. Chai, Y.W. Dong, N. Gauvin, W. Hajdas, M. Kole, M.N. Kong, R. Kramert, L. Li, J.T. Liu, X. Liu, R. Marcinkowski, S. Orsi, M. Pohl, D. Rapin, D. Rybka, A. Rutczynska, H.L. Shi, P. Socha, J.C. Sun, L.M. Song, J. Szabelski, I. Traseira, H.L. Xiao, R.J. Wang, X. Wen, B.B. Wu, L. Zhang, L.Y. Zhang, S.N. Zhang, Y.J. Zhang, and A. Zwolinska. Design and construction of the polar detector. *Nuclear Instruments and Methods in Physics Research Section A: Accelerators, Spectrometers, Detectors and Associated Equipment*, 877:259–268, January 2018.

[2] Nicolas Produit, Merlin Kole, Xin Wu, Nicolas De Angelis, Hancheng Li, Dominik Rybka, Agnieszka Pollo, Slawomir Mianowski, Jochen Greiner, J Michael Burgess, Jianchao Sun, and Shuang-Nan Zhang. Polar-2, the next generation of grb polarization detector. In *Proceedings of 38th International Cosmic Ray Conference — PoS(ICRC2023)*, ICRC2023, page 550. Sissa Medialab, August 2023.

[3] Johannes Hulsman. POLAR-2: a large scale gamma-ray polarimeter for GRBs. In Jan-Willem A. den Herder, Shouleh Nikzad, and Kazuhiro Nakazawa, editors, *Space Telescopes and Instrumentation 2020: Ultraviolet to Gamma Ray*, volume 11444, page 114442V. International Society for Optics and Photonics, SPIE, 2020.

[4] Nicolas De Angelis. *Development of the next generation space-based compton polarimeter and energy resolved polarization analysis of gamma-ray bursts prompt emission*. PhD thesis, Université de Genève, 2023.

[5] Merlin Kole, Nicolas De Angelis, Nicolas Produit, Franck Cadoux, Yannick Favre, Jochen Greiner, Johannes Hulsman, Sebastian Kusyk, Hancheng Li, Dominik Rybka, Jerome Stauffer, Adrien Stil, Jianchao Sun, Jan Swakon, Damian Wrobel, and Xin Wu. Design and performance of a universal sipm readout system for x- and gamma-ray missions. *Nuclear Instruments and Methods in Physics Research Section A: Accelerators, Spectrometers, Detectors and Associated Equipment*, 1080:170782, November 2025.

[6] Nicolas De Angelis. Temperature loop correction of the SiPM bias, May 2024. Internal POLAR-2 document.

[7] https://svn.astro.unige.ch/rp1-polar-2.

[8] Adam Nepomuk Otte, Distefano Garcia, Thanh Nguyen, and Dhruv Purushotham. Characterization of three high efficiency and blue sensitive silicon photomultipliers. *Nuclear Instruments and Methods in Physics Research Section A: Accelerators, Spectrometers, Detectors and Associated Equipment*, 846:106–125, 2017.